Automated CT-FFR model for diagnosing hemodynamically significant coronary artery disease. A prospective validation study.

Authors:

Anders T. Bråten[a,b] MD.

Fredrik E. Fossan[c] PhD.

Lucas O. Muller[d] PhD.

Arve Jørgensen[b,e] MD, PhD.

Knut H. Stensæth[b,e] MD, PhD.

Leif R. Hellevik[c] PhD.

Rune Wiseth[a,b] MD, PhD.

[a]Clinic of Cardiology, St.Olavs University Hospital, Norway

[b]Department of Circulation and Medical Imaging, Norwegian University of Science and Technology, Norway

[c]Department of Structural Engineering, Norwegian University of Science and Technology, Norway

[d]Department of Mathematics, University of Trento, Italy

[e]Department of Radiology and Nuclear Medicine, St.Olavs University Hospital, Norway

Funding: The Liaison Committee for education, research and innovation in Central Norway.

Conflict of interest: None.

Corresponding author:

Anders Tjellaug Bråten, Clinic of Cardiology, St. Olavs University Hospital

Po 3250 Torgarden

NO 7006 Trondheim, Norway

E-mail: anders.tjellaug.braten@stolav.no

Phone: +47 72820326

Abstract

Aims

To assess the diagnostic performance of a novel computed tomography-derived fractional flow reserve (CT-FFR) algorithm and to compare its accuracy at three predefined sites: a) at the location of invasive fractional flow reserve (FFR) measurements ($CT\text{-}FFR_{atloc}$), b) at selected sites determined by an automated module integrated within the algorithm ($CT\text{-}FFR_{auto}$), and c) distally in the vessel ($CT\text{-}FFR_{distal}$).

Methods and results

We prospectively recruited 108 consecutive patients with stable symptoms of coronary artery disease (CAD) and at least one suspected obstructive lesion on coronary computed tomography angiography (CCTA). CT-FFR was validated against invasive FFR as gold standard using an FFR≤ 0.80 to define myocardial ischemia. $CT\text{-}FFR_{atloc}$ showed good correlation with invasive FFR (r=0.67) and improved the ability to detect myocardial ischemia compared to CCTA at both lesion (AUC 0.83 vs 0.65, P<0.001) and patient level (AUC 0.87 vs 0.74, P=0.007). $CT\text{-}FFR_{auto}$ demonstrated similar diagnostic accuracy to $CT\text{-}FFR_{atloc}$ and significantly improved specificity compared to $CT\text{-}FFR_{distal}$ (86% vs 49%, P<0.001). High end CT quality improved the diagnostic performance of $CT\text{-}FFR_{auto}$, demonstrating an AUC of 0.92, similarly, the performance was improved in patients with low-to-intermediate CAC score with an AUC of 0.88.

Conclusion

Implementing an automated module to determine the site of CT-FFR evaluations was feasible and $CT\text{-}FFR_{auto}$ demonstrated comparable diagnostic accuracy to $CT\text{-}FFR_{atloc}$ when assessed against invasive FFR. Both $CT\text{-}FFR_{atloc}$ and $CT\text{-}FFR_{auto}$ improved the diagnostic performance

compared to CCTA and improved specificity compared to CT-FFR_{distal}. High end CT quality and low-to-intermediate calcium burden improved the diagnostic performance of our algorithm.

ClinicalTrials.gov id: NCT03045601

Introduction

Current guidelines recommend coronary computed tomography angiography (CCTA) as a first-line diagnostic test in symptomatic patients with low to moderate clinical likelihood of coronary artery disease (CAD) (1). The presence and extent of coronary atherosclerosis has prognostic value and is important for further medical treatment (2). More controversial, however, is the selection of patients for invasive coronary angiography (ICA) based on CCTA alone. The stenosis degree on CCTA correlates well with ICA results but is unreliable as a marker for ischemia and tends to overestimate the physiological severity of coronary stenoses when compared to fractional flow reserve (FFR) (3).

Computed tomography derived fractional flow reserve (CT-FFR) is a novel technology that provides a noninvasive estimate of FFR, which relies on computational fluid dynamics and vessel geometry extracted from CCTA. The fluid dynamics equations used to calculate the pressure gradients over atherosclerotic lesions, also calculate the progressive decline in pressure gradients in healthy, continuously tapering vessels irrespective of coronary stenosis. The diagnostic performance of the test using a dichotomous cut off value of 0.80 for defining ischemia will therefore not only depend on stenosis degree and flow, but also on the site of the CT-FFR evaluations.

Traditionally, validation studies of CT-FFR have relied on information from the ICA, in which CT-FFR values are obtained at the exact position of the invasive measurements (4). In a clinical setting, this information is unavailable and studies on clinical outcome have applied CT-FFR values from the distal end of each coronary distribution to define myocardial ischemia (5). Recent studies have shown that the diagnostic accuracy of CT-FFR improves when obtained directly distal to the lesion, rather than distally in the vessel (6, 7). Additionally, consensus

papers have advised caution in using CT-FFR values from the distal end and emphasized the importance of evaluating the presence of relevant pathology upstream on both CCTA and CT-FFR (8). However, this approach requires subjective judgement and makes the selection of proper location of CT-FFR predictions dependent on the experience and training of the reading physician.

The purpose of the present study was to validate a novel CT-FFR approach that incorporates a module that automatically defines the site for CT-FFR predictions and to compare the diagnostic performance of CT-FFR estimated at three different sites within the vessel.

Methods

Study design and population

Between October 2018 and March 2021, we prospectively enrolled 108 consecutive patients with stable chest pain and at least one suspected significant stenosis (visually ≥50% stenosis diameter) on CCTA referred for a clinically indicated ICA. Exclusion criteria included previous coronary revascularization, age >75 years, body mass index >40, hospitalization for unstable CAD after CCTA, non-diagnostic CCTA quality, and contraindications to adenosine. Patients with clinically significant arrhythmia, cardiomyopathy, congenital coronary anomaly, chronic total occlusions, coronary aneurysms, or significant valvular heart disease were ineligible. Assessment during recruitment included a complete echocardiographic examination. Patients with bifurcation lesions, ostial stenosis and serial lesions were considered eligible. For serial stenoses, we considered only one pressure measurement per vessel, specifically the most distal. The study protocol was approved by the Regional Ethics Committee of Central Norway (2016/1609),

registered at the clinicaltrials.gov id; NCT03045601 and performed according to the Declaration of Helsinki. Written informed consent was obtained from all participants.

CT imaging

CCTA was conducted at St. Olavs university hospital and at five collaborating local hospitals. A total of nine CT scanners from three different vendors were employed: General Electric Healthcare (Waukesha, WI, USA), Siemens Healthineers (Erlangen, Germany), and Philips Healthcare (Best, Netherlands). The scanners used included four GE Revolution DE 256-slice scanners with a 160-mm detector width, one GE Discovery 64-slice scanner with a 40-mm detector width, two Somatom Flash DE 2 × 128-slice scanners with a 2 × 38-mm detector width and one Philips iCT 256-slice scanner with an 80-mm detector width. Image acquisition and post-processing was performed according to current guidelines (9). Beta -blockers were administered orally and if necessary, intravenously to reach a target heart rate of <60 bpm. Sublingual nitroglycerin was administered before scanning in all patients. Local radiology readers evaluated the CCTA images according to guidelines and referred to ICA in cases with presence of one or more suspected obstructive lesions (10). CCTA datasets were post processed in syngo.via software (version VB40 and VB60, Siemens Healthcare GmbH, Erlangen, Germany) and re-evaluated separately by two radiologists. Both radiologists were blinded to ICA results, invasive FFR and CT-FFR results. Stenosis degree was quantified in all coronary segments with diameter >1.5 mm and stenoses ≥50% were considered significant. Coronary Artery Calcium score (CAC score) was calculated according to guidelines (11). A CAC score below 300 represented the low-to-intermediate category, while a CAC score of 300 or higher indicated the high CAC score category, following current recommendations (12) .

Invasive coronary angiography

ICA was performed within three months following CCTA using standard techniques. Invasive FFR measurements were performed in all stenoses documented by CCTA and confirmed through the invasive procedure. FFR measurements were not carried out in cases where invasive coronary angiography did not reveal any evidence of stenosis, i.e. blooming artifacts, or in subtotal stenoses that were not amendable to invasive pressure measurements. Additional FFR measurements were conducted in cases of intermediate stenoses with questionable hemodynamic significance not identified by CCTA.

Fractional flow measurements

FFR was measured using Verrata Plus (Philips Volcano, San Diego, USA) pressure wires according to standard practice. Intracoronary nitroglycerine (0.2 mg) was administered to all patients before advancing the pressure wire into the coronary artery and hyperemia was induced by continuous intravenous infusion of adenosine at a rate of 140 µg/kg/min. FFR was defined as the lowest observed value and the precise positions of FFR measurements were recorded for each patient. Following the measurements, the pressure wire was retracted to the equalization point at the tip of the guiding catheter to ensure there was no drift. Acceptable drift was defined as ±0.02. Positive FFR was defined as ≤0.80, indicating myocardial ischemia.

CT-FFR

We employed a previously presented machine learning-augmented reduced order model to predict pressure and flow distribution in the coronary tree (13-15). For each patient a 3D arterial model of both coronary vessels was generated semi-automatically using Mimics (Materialise, Leuven, Belgium). Successively, we extracted centerlines from the 3D segmentations and

sampled radius data at intervals of approximately 0.125 mm, facilitating the creation of a cross-sectional area profile. A steady state 1D Navier-Stokes equation was used to provide a physics-based estimate of the pressure losses in healthy regions of the coronary tree. This estimate, along with geometrical data and information on upstream dynamics, served as input features for a neural network, which computed the pressure losses in these regions. To compute pressure drops in stenotic segments, we had to account for dissipative effects due to laminar flow disruption by using a reduced-order physics-based model in combination with a neural network, which was trained to incorporate 3D fluid dynamical effects. The pressure solution was used to calculate CT-FFR in all coronary vessels (Figure 1) and has been previously validated against a 3D algorithm in stable CAD patients (13). For the baseline simulation, the total coronary flow was derived from the mass of the left ventricle, assuming normal perfusion values. Total flow was then distributed among terminal vessels according to estimates of the myocardial mass supplied by each vessel, performed using a Voronoi algorithm. The simulation allowed to compute the resting peripheral resistances from the flows and pressures of the terminal vessels. Hyperemia was simulated by reducing the resting peripheral resistance, incorporating a factor that accounts for autoregulatory mechanisms responding to variations in trans-stenotic pressure gradients across coronary stenoses. The operators performed the CT-FFR analysis on a standard desktop computer and were blinded to all clinical information, CCTA results, ICA and FFR results. Total processing time was approximately one hour, with the majority of the time (~59 minutes) dedicated to creating the 3D models of the coronary arteries and the left ventricle. The actual solver time for $CT\text{-}FFR_{auto}$ with the available 3D models was less than one minute.

Location of CT-FFR predictions

In this study, CT-FFR evaluation was performed on all lesions identified on CCTA and ICA, for which FFR was measured invasively. We considered three different CT-FFR evaluation locations:

FFR measurement locations (CT-FFR$_{atloc}$)

CT-FFR$_{atloc}$ was computed by evaluating CT-FFR at the specified site of the invasive FFR measurement location. This location was shared in a 3D model of the coronary vessels after the final CT-FFR simulations were completed.

Distal locations (CT-FFR$_{distal}$)

Given a lesion for which invasive FFR was available, CT-FFR$_{distal}$ was computed by evaluating CT-FFR at the respective distal location to the lesion of interest. The distal location corresponded to the most distal point of the vessel of interest, excluding diameters smaller than 1.8 mm.

Automatically selected locations (CT-FFR$_{auto}$)

We sought to validate a fully automated algorithm to determine sites for CT-FFR evaluation, to avoid potential biases and subjective interpretations of CT-FFR results. This algorithm uses coronary geometry and continuous CT-FFR data as inputs and integrates clinically relevant geometrical and functional criteria to determine CT-FFR values corresponding to a stenosis. Specifically, the evaluation encompassed all major coronary paths, ranging from the ostium to all regions where the vessel diameter was larger than 1.8 mm. The stenosis detection was fully automated, involving a distal-to-proximal search. For a stenosis to be selected, two criteria had to

be satisfied, one geometric and the other functional. A stenosis was considered of geometric significance if the stenosis degree was greater than 25%. This assessment was based on the vessel radius obtained from 3D segmentations, compared to a predicted, reconstructed baseline normal vessel radius. In turn, the functional significance criterion, required a change in ΔCT-FFR greater than 0.1 over a 20 mm segment of the vessel. After a stenosis fulfilling these two criteria was identified, CT-FFR was evaluated at the distal end of the stenosis, as illustrated in Figure 2.

Statistics

All data analyses was performed using SPSS version 28.0.1.0 (Armonk, NY: IBM Corp) and MedCalc® statistical software version 20.110 (Medcalc Software Ltd, Ostend, Belgium). Categorical data are reported as frequency and percentages, and continuous variables as means ± standard deviations. Diagnostic accuracy, specificity, sensitivity, PPV and NPV were calculated with a 95% confidence interval using CCTA with a stenosis diameter ≥50% and CT-FFR with a cut off limit of ≤0.80 indicating hemodynamic significance. Accuracy, specificity, and sensitivity were compared using McNemar's test with a P value of <0.05 considered statistically significant. Correlations between CT-FFR predictions and invasively measured FFR were assessed using the Pearson correlation coefficient at lesion level and agreement between calculated and measured values were assessed by Bland-Altman analyses estimating 95% limits of agreement. Receiver operating characteristics curves with areas under the curve were estimated with a 95% confidence interval and compared using the method of DeLong.

Results

Baseline characteristics

In total, 108 patients with 175 lesions evaluated with intracoronary FFR measurements were included for analysis. Additionally, 13 vessels with eccentric plaque and blooming artifacts on CCTA were classified as non-stenotic during invasive angiography, as no visual stenosis was observed, and FFR measurements were not performed. These were subsequently included as dichotomously negative lesions. Moreover, nine lesions with subtotal occlusions with diameter stenosis >90% without pressure measurements were included, and dichotomously defined as positive lesions. Patient and vessel characteristics are presented in table 1 and table 2. Mean age of the population was 62 ±8 years and 67% were men. The pretest probability of obstructive CAD was low to intermediate, 23 ±12 % according to the 2019 ESC guidelines of chronic coronary syndrome (1). All but two CT examinations were prospectively gated with a mean effective radiation dose of 5.1 ±5.8 mSv (conversion factor 0.026). Time from CCTA to ICA was 35 ±15 days. Fifty-three (49%) patients had at least one FFR measurement indicating ischemia (FFR ≤0.80), 19 (18%) patients had functional multivessel disease. Forty-five patients (42%) were revascularized with PCI or CABG. On a per lesion level the prevalence of hemodynamically significant stenosis was 42%. The mean FFR was 0.79 ±0.13 and mean CT-FFR at the site of invasive FFR measurement location ($CT\text{-}FFR_{atloc}$) was 0.82 ±0.13. The prevalence of positive $CT\text{-}FFR_{atloc}$ predictions at patient level was 46% (50/108) and the prevalence of positive $CT\text{-}FFR_{auto}$ was 42% (45/108). CCTA and $CT\text{-}FFR_{distal}$ were both positive in 73% (79/108).

CT-FFR$_{atloc}$ and invasive FFR at lesion level

The Bland Altman analysis of CT-FFR$_{atloc}$ demonstrated a mean difference of -0.03 indicating that CT-FFR$_{atloc}$ marginally underestimated the hemodynamic significance of lesions when compared to invasive FFR with limits of agreement between -0.22 to 0.17. However, the differences between CT-FFR and FFR values were dependent on the hemodynamic significance of the stenosis, with wider limits of agreement in hemodynamically significant stenoses. Pearson correlation coefficient was 0.67 (95% CI 0.57-0.74, P <0.001,) indicating a significant and moderately strong positive correlation between CT-FFR$_{atloc}$ and FFR measurements (Figure 3).

Overall diagnostic performance of CCTA, CT-FFR$_{atloc}$, CT-FFR$_{auto}$ and CT-FFR$_{distal}$ at lesion and patient level (Figure 4/ Table 3)

The area under the curve (AUC) of the receiver operating characteristics for identifying hemodynamic significant stenoses at the lesion level was 0.83 for CT-FFR$_{atloc}$, 0.81 for CT-FFR$_{auto}$, 0.78 for CT-FFR$_{distal}$ and 0.65 for CCTA alone. When considering patient level analysis, the AUC for CT-FFR$_{atloc}$ was 0.87, for CT-FFR$_{auto}$ 0.86 and for CT-FFR$_{distal}$ 0.83. In comparison, CCTA alone had an AUC of 0.74. At lesion level CT-FFR$_{atloc}$ improved the ability to detect hemodynamically significant CAD compared to both CCTA (P <0.001) and CT-FFR$_{distal}$ (P =0.016). Compared to CT-FFR$_{auto}$, the discriminatory value was comparable (P =0.457). Similarly, on patient level there was no significant difference between CT-FFR$_{auto}$ and CT-FFR$_{atloc}$ (AUC 0.87 vs 0.86), and both improved the discriminatory power to detect ischemia compared to CCTA (P =0.015 and P =0.007, respectively). The ability to identify ischemia using CT-FFR$_{distal}$ was not significantly increased when compared to CCTA alone (P =0.067).

Diagnostic accuracy, sensitivity and specificity of CT-FFR$_{atloc}$, CT-FFR$_{auto}$ and CT-FFR$_{distal}$ for the diagnosis of ischemia (Figure 5/ Table 3)

At lesion level the diagnostic accuracy of CT-FFR$_{atloc}$ was 78%, with a specificity of 89% and sensitivity of 64%. At the patient level the corresponding values were 81% for accuracy, 84% for specificity and 77% for sensitivity. For CT-FFR$_{auto}$ at lesion level, the diagnostic accuracy was 76%, specificity was 91% and sensitivity 54% and at patient level accuracy was 78%, specificity 86% and sensitivity 70%. At patient level, both diagnostic specificity and accuracy of CT-FFR$_{atloc}$ was improved compared to CCTA, 84% vs 40% (P <0,001) and 81% vs 63% (P =0.004), respectively. The specificity of CT-FFR$_{atloc}$ and CT-FFR$_{auto}$ was significantly improved compared to both CCTA and CT-FFR$_{distal}$ at both lesion and patient level (P <0.001). A model which always predicts the most frequent class is commonly denoted a no-information rate (NIR) model. When the accuracy of CT-FFR$_{atloc}$ and CT-FFR$_{auto}$ were evaluated against the NIR model, both showed a significant statistical improvement, with P-values of <0.01. The accuracy of CT-FFR$_{distal}$ was also statistically improved compared to NIR (P =0.013), in contrast to the accuracy of CCTA which was not significantly improvement over the NIR model (P =0.177).

Impact of image quality on CT-FFR$_{auto}$

Coronary calcium: Of 108 patients, 66 (61%) had CT scans available for CAC scoring. ROC curve analysis revealed a higher discriminative power of CT-FFR$_{auto}$ to detect hemodynamically significant CAD in patients with a low-to-intermediate CAC score (Agatston score <300) with an AUC of 0.88 (95% CI 0.74-0.97). In contrast, the performance was more moderate in the high CAC score group (Agatston score ≥300), with an AUC of 0.62 (95% CI 0.42-0.79). On a per patient level, the accuracy, specificity and sensitivity of CT-FFR$_{auto}$ were 87%, 92% and 79%, respectively, in the low-to-intermediate CAC score group, compared to 50%, 63% and 45%,

respectively, in the high CAC score group. With a prevalence of 37% in the low-to-intermediate CAC group and 71%, in the high CAC group, the NIR-model would predict all patients in the low-to intermediate CAC group to be healthy and all patients in the high CAC group to be ischemic. The accuracy of CT-FFR_{auto} was significantly better when compared to the NIR model in the low-to-intermediate CAC score group (P=0.022). However, this was not statistically significant in the high CAC score group (P =0.210).

Despite the decrease in specificity and sensitivity in the high CAC score group, the PPV remained consistent with a PPV of 85% at patient level in the low-to-intermediate group, and 88% in the high CAC score group. The PPV at per lesion level was 82% in the low-to-intermediate group and 81% in the high CAC group. The per patient and per lesion level PPV and NPV are presented in Figure 6.

CT scanner technology: In four out of six centers, and for 55 (51%) patients, CT scans were conducted using a GE Revolution scanner, which represents more advanced CT technology compared to the older scanners used in this study. The discriminative power of CT-FFR_{auto} in identifying hemodynamically significant CAD in scans acquired using this upgraded and contemporary CT technology, showed improved performance, with an AUC of 0.92 (95% CI 0.82-0.98) and an accuracy of 85%, specificity of 90% and sensitivity of 81%. Conversely, for scans acquired with the remaining CT scanners, the analysis revealed a diminished AUC of 0.80 (95% CI 0.66-0.89), with corresponding accuracy, specificity and sensitivity of 70%, 81% and 59%, respectively.

Discussion

In this study we validated the diagnostic accuracy of a novel CT-FFR algorithm that uses reduced order modeling to evaluate the hemodynamically significance of CAD. A unique aspect of this study was the comparison of the algorithm's diagnostic performance at three predetermined locations for CT-FFR predictions. These locations included the site of invasive FFR measurements, the lowest value distally in the vessel, and a site specified by a fully automated module that gives predictions directly distal to lesions of interest.

CT-FFR_{atloc} correlated well with invasive FFR and showed improved diagnostic performance with high accuracy and specificity compared to CCTA. Our findings align with and are comparable to other validation studies using machine-learning algorithms and reduced order models showing low systematic bias and moderately narrow limits of agreement (16).

We also demonstrated the feasibility of implementing an automated module to define the site of CT-FFR evaluations where CT-FFR_{auto} proved to be non-inferior to CT-FFR_{atloc} and reduced the number of false positive results compared to CT-FFR_{distal}. From a clinical point of view, this is reassuring as this algorithm matches best with the clinical guidance of CT-FFR and underscores the importance of location in CT-FFR evaluations (8).

Moreover, data showed a notable difference in the accuracy of CT-FFR with increasing calcium burden, that aligns with earlier studies, and that the performance improves significantly when using high end CT technology (17).

Over the past two decades, CCTA has evolved significantly, and is now considered a first-line test for evaluating patients with chest pain and suspected stable CAD. Additionally, guidelines have provided CT-FFR a class 2a recommendation in patients with intermediate lesions on

CCTA, recognizing its potential to improve specificity and reduce unnecessary ICA (18). The recommendations are based on validation studies demonstrating improved specificity and reduced false positive rate compared to CCTA alone (4). However, in most studies the extracted CT-FFR values were dependent on knowledge of FFR wire position and therefore not fully blinded to invasive information. Several trials have highlighted the importance of the CT-FFR evaluation site and there is growing evidence that distal CT-FFR values introduce a high false positive rate compared to invasive FFR (7). An investigation by Cami et al. found that CT-FFR values obtained at the end of the vessel significantly overestimated the hemodynamic significance of coronary lesions with a high number of false positive results and a specificity of 50%. The study also revealed that the specificity improved to 86% when evaluated 2 cm distal to the target lesion, which closely mirrors our CT-FFR_{auto} results (6). Several factors may explain the observed overestimation of hemodynamic significance by CT-FFR at the distal end of the vessel compared to predictions made directly after the lesion. It is noteworthy that a gradual decrease of intracoronary pressure along the length of the epicardial arteries is also observed during invasive FFR measurements, particularly in vessels with non-obstructive and diffuse coronary artery disease (19). However, this phenomenon is less pronounced with invasive FFR than with CT-FFR (20). In addition, calculations involved in CT-FFR predictions introduce a gradually decreasing pressure gradient due to the continuously reduction in vessel dimension. This is in line with Poiseuille's law that states that the pressure drop is inversely proportional to the fourth power of the diameter and linearly related to the vessel length and flow through the vessel. Furthermore, the limited resolution of CCTA may also contribute by overestimating flow rates in distal segments, as small side branches may be neglected, and by introducing artificial stenoses, particularly in distal regions where dimensions, image noise and low concentration of

contrast may obscure true anatomy and potentially lead to false positive results. To address these challenges, our algorithm implemented a fully automated module that employed both a geometric and functional criterion to accurately detect relevant stenoses and make the CT-FFR predictions directly distal to them. This integrated strategy ensured that stenoses with diameter narrowing exceeding 25% were identified during computer simulations and evaluated for functional relevance as studies have revealed that among lesions within the range of 30-50%, one-third is hemodynamically significant (21). By incorporating the functional criterion, the module would detect hemodynamically significant stenosis that would have been missed by an anatomical evaluation alone if using the standard cut-off limit of 50%. The utilization of ΔCT-FFR over a 2 cm segment also served a purpose to ensure the detection of relative focal disease that may require invasive therapy and help differentiate such lesions from more diffuse atherosclerosis or healthy vessels that gradually taper. The subanalysis of the impact of image quality on CT-FFR_{auto} highlights the importance of accurate vessel geometry for CT-FFR predictions and underscores the vulnerability to imprecise anatomical inputs, particularly in patients with reduced image quality due to high calcium burden. Previous studies have analyzed the effect of CAC score on CT-FFR and reported moderate PPV levels across all CAC score ranges (22). In contrast, in our study the PPV of CT-FFR_{atloc} and CT-FFR_{auto} was rather unaffected by CAC score, remaining higher (~80%) than values previously reported. However, the NPV for CT-FFR_{atloc} and CT-FFR_{auto} was significantly reduced in the high CAC score group. Conversely, the NPV remained consistently high for CT-FFR_{distal} and CCTA while their PPV was more affected by the CAC score and remained lower than the PPV of CT-FFR_{atloc} and CT-FFR_{auto}. This suggests that the impact of the CAC score on the diagnostic performance of CT-FFR is dependent on the site of evaluation. In particular it suggests that CT-FFR_{auto} is less

applicable to patients with high calcium burden. Conversely, the increase in diagnostic performance points to the potential of CT-FFR_{auto} as CT scanner technology continuous to improve, raising expectations for the method as technological advances progress.

Limitations

There are several limitations to consider. While the number of patients included is limited, it aligns with other studies of similar design. Despite encouraging results, further large-scale, prospective studies are needed to improve generalizability and statistical robustness. Total occlusions were omitted since invasive pressure measurements, could not be reliably obtained, and varying degrees of collateral flow could influence FFR values in the other vessels. Significant valvular disease, such as aortic stenosis, were also excluded, as these conditions may impact various physiological parameters and potentially lead to underestimating the functional severity of coronary stenoses. Furthermore, the physiological assumptions underlying the CT-FFR algorithm may not apply to these patients. A subanalysis on the significance of calcium burden, despite a relatively small sample size, highlighted the importance of reliable geometric reconstructions from the CT scans. Despite notable numerical differences in diagnostic performance between the low-to-moderate CAC score group and the high CAC score group, statistical significance was not achieved, probably due to limited statistical power.

While the processing time of the computer algorithm is short, the vessel segmentation and development of the 3D anatomical model are time consuming and with challenges of reproducibility. To address this, developing and integrating an automated segmentation tool to reduce reliance on manual corrections will be a central focus of further work.

Invasive FFR measurements were performed at only one location for each lesion, with wire positioning selected at the discretion of the interventionist and not consistently at the distal end of the vessel. This makes it challenging to determine how much of the pressure loss in distal segments is due to physiological factors and how much is introduced by CT-FFR as a method and due to modelling choices.

In this study, only one operator analyzed CT-FFR, preventing the assessment of interrater reliability. However, aside from uncertainties and variability in the geometric reconstruction of the coronary arteries, the algorithm operates independently of user input, and thereby provide perfect reproducibility.

Conclusion

CT-FFR using an automated module to determine the site of CT-FFR evaluations provided comparable diagnostic accuracy as CT-FFR estimated at the location of invasive FFR measurements when evaluated against invasive FFR. Both improved diagnostic performance compared to CCTA, and improved specificity particularly in contrast to CT-FFR estimated distally in the vessel. The study demonstrates the potential of CT-FFR to reduce unnecessary ICA in patients with stable angina but underscores the importance of location of CT-FFR predictions. The implementation of an automated module for determining the site of CT-FFR evaluations was feasible but is dependent on calcium burden and improves when using high end CT technology. Further studies are warranted to determine its utility in clinical decision-making.

Acknowledgements: The authors would like to thank Bjørn Inge Våga, Olav Magne Leiren, Matthias Heigert and Ola Kleveland for their support in performing the invasive FFR measurements.

Data availability statement

Data are available from the corresponding author on reasonable request.

References

1. Knuuti J, Wijns W, Saraste A, Capodanno D, Barbato E, Funck-Brentano C, et al. 2019 ESC Guidelines for the diagnosis and management of chronic coronary syndromes. Eur Heart J. 2020;41(3):407-77.
2. Investigators S-H, Newby DE, Adamson PD, Berry C, Boon NA, Dweck MR, et al. Coronary CT Angiography and 5-Year Risk of Myocardial Infarction. N Engl J Med. 2018;379(10):924-33.
3. Knuuti J, Ballo H, Juarez-Orozco LE, Saraste A, Kolh P, Rutjes AWS, et al. The performance of non-invasive tests to rule-in and rule-out significant coronary artery stenosis in patients with stable angina: a meta-analysis focused on post-test disease probability. Eur Heart J. 2018;39(35):3322-30.
4. Norgaard BL, Leipsic J, Gaur S, Seneviratne S, Ko BS, Ito H, et al. Diagnostic performance of noninvasive fractional flow reserve derived from coronary computed tomography angiography in suspected coronary artery disease: the NXT trial (Analysis of Coronary Blood Flow Using CT Angiography: Next Steps). J Am Coll Cardiol. 2014;63(12):1145-55.
5. Douglas PS, De Bruyne B, Pontone G, Patel MR, Norgaard BL, Byrne RA, et al. 1-Year Outcomes of FFRCT-Guided Care in Patients With Suspected Coronary Disease: The PLATFORM Study. J Am Coll Cardiol. 2016;68(5):435-45.
6. Cami E, Tagami T, Raff G, Gallagher MJ, Fan A, Hafeez A, et al. Importance of measurement site on assessment of lesion-specific ischemia and diagnostic performance by coronary computed tomography Angiography-Derived Fractional Flow Reserve. J Cardiovasc Comput Tomogr. 2021;15(2):114-20.
7. Omori H, Hara M, Sobue Y, Kawase Y, Mizukami T, Tanigaki T, et al. Determination of the Optimal Measurement Point for Fractional Flow Reserve Derived From CTA Using Pressure Wire Assessment as Reference. AJR Am J Roentgenol. 2021;216(6):1492-9.
8. Norgaard BL, Fairbairn TA, Safian RD, Rabbat MG, Ko B, Jensen JM, et al. Coronary CT Angiography-derived Fractional Flow Reserve Testing in Patients with Stable Coronary Artery Disease: Recommendations on Interpretation and Reporting. Radiol Cardiothorac Imaging. 2019;1(5):e190050.
9. Abbara S, Blanke P, Maroules CD, Cheezum M, Choi AD, Han BK, et al. SCCT guidelines for the performance and acquisition of coronary computed tomographic angiography: A report of the society of Cardiovascular Computed Tomography Guidelines Committee: Endorsed by the North American Society for Cardiovascular Imaging (NASCI). J Cardiovasc Comput Tomogr. 2016;10(6):435-49.

10. Leipsic J, Abbara S, Achenbach S, Cury R, Earls JP, Mancini GJ, et al. SCCT guidelines for the interpretation and reporting of coronary CT angiography: a report of the Society of Cardiovascular Computed Tomography Guidelines Committee. J Cardiovasc Comput Tomogr. 2014;8(5):342-58.
11. Hecht HS, Cronin P, Blaha MJ, Budoff MJ, Kazerooni EA, Narula J, et al. 2016 SCCT/STR guidelines for coronary artery calcium scoring of noncontrast noncardiac chest CT scans: A report of the Society of Cardiovascular Computed Tomography and Society of Thoracic Radiology. J Cardiovasc Comput Tomogr. 2017;11(1):74-84.
12. Cury RC, Leipsic J, Abbara S, Achenbach S, Berman D, Bittencourt M, et al. CAD-RADS 2.0 - 2022 Coronary Artery Disease - Reporting and Data System.: An expert consensus document of the Society of Cardiovascular Computed Tomography (SCCT), the American College of Cardiology (ACC), the American College of Radiology (ACR) and the North America Society of Cardiovascular Imaging (NASCI). J Am Coll Radiol. 2022;19(11):1185-212.
13. Fossan FE, Muller LO, Sturdy J, Braten AT, Jorgensen A, Wiseth R, et al. Machine learning augmented reduced-order models for FFR-prediction. Computer Methods in Applied Mechanics and Engineering. 2021;384.
14. Muller LO, Fossan FE, Braten AT, Jorgensen A, Wiseth R, Hellevik LR. Impact of baseline coronary flow and its distribution on fractional flow reserve prediction. Int J Numer Method Biomed Eng. 2019:e3246.
15. Fossan FE, Sturdy J, Muller LO, Strand A, Braten AT, Jorgensen A, et al. Uncertainty Quantification and Sensitivity Analysis for Computational FFR Estimation in Stable Coronary Artery Disease. Cardiovasc Eng Technol. 2018;9(4):597-622.
16. Coenen A, Kim YH, Kruk M, Tesche C, De Geer J, Kurata A, et al. Diagnostic Accuracy of a Machine-Learning Approach to Coronary Computed Tomographic Angiography-Based Fractional Flow Reserve: Result From the MACHINE Consortium. Circ Cardiovasc Imaging. 2018;11(6):e007217.
17. Tesche C, Otani K, De Cecco CN, Coenen A, De Geer J, Kruk M, et al. Influence of Coronary Calcium on Diagnostic Performance of Machine Learning CT-FFR: Results From MACHINE Registry. JACC Cardiovasc Imaging. 2020;13(3):760-70.
18. Gulati M, Levy PD, Mukherjee D, Amsterdam E, Bhatt DL, Birtcher KK, et al. 2021 AHA/ACC/ASE/CHEST/SAEM/SCCT/SCMR Guideline for the Evaluation and Diagnosis of Chest Pain: Executive Summary: A Report of the American College of Cardiology/American Heart Association Joint Committee on Clinical Practice Guidelines. Circulation. 2021;144(22):e368-e454.
19. De Bruyne B, Hersbach F, Pijls NH, Bartunek J, Bech JW, Heyndrickx GR, et al. Abnormal epicardial coronary resistance in patients with diffuse atherosclerosis but "Normal" coronary angiography. Circulation. 2001;104(20):2401-6.
20. Cami E, Tagami T, Raff G, Fonte TA, Renard B, Gallagher MJ, et al. Assessment of lesion-specific ischemia using fractional flow reserve (FFR) profiles derived from coronary computed tomography angiography (FFRCT) and invasive pressure measurements (FFRINV): Importance of the site of measurement and implications for patient referral for invasive coronary angiography and percutaneous coronary intervention. J Cardiovasc Comput Tomogr. 2018;12(6):480-92.
21. Curzen N, Rana O, Nicholas Z, Golledge P, Zaman A, Oldroyd K, et al. Does routine pressure wire assessment influence management strategy at coronary angiography for diagnosis of chest pain?: the RIPCORD study. Circ Cardiovasc Interv. 2014;7(2):248-55.
22. Chiou A, Hermel M, Sidhu R, Hu E, van Rosendael A, Bagsic S, et al. Artificial intelligence coronary computed tomography, coronary computed tomography angiography using fractional flow reserve, and physician visual interpretation in the per-vessel prediction of abnormal invasive adenosine fractional flow reserve. Eur Heart J Imaging Methods Pract. 2024;2(1):qyae035.

Figure legends:

Graphical abstract.

Figure 1. Case example.

A patient with exertional dyspnea and atypical chest pain with an intermediate stenosis in the proximal left anterior descending artery on CCTA (A, red arrow). ICA, revealed a moderate stenosis (B, blue arrow) with an FFR of 0.89 (D, green arrow), indicating a hemodynamically non-significant lesion. The predicted CT-FFR (C) at the location of invasive FFR measurement was 0.86 ($CT\text{-}FFR_{atloc}$). CT-FFR was 0.87 at the site selected automatically directly distal to the lesion ($CT\text{-}FFR_{auto}$). In contrast, the distal CT-FFR ($CT\text{-}FFR_{distal}$) indicated ischemia with a predicted value of 0.68. Figure D, lower left corner, pressure curve of invasive FFR.

Figure 2. Determination of $CT\text{-}FFR_{auto}$ measurements.

To determine lesion-specific $CT\text{-}FFR_{auto}$, both a functional and anatomical criterion had to be met. The functional criterion involves a ΔCT-FFR of more than 0.1 over a 20 mm segment, while the anatomical criterion requires diameter stenosis greater than 25%. When both criteria are met, a relevant stenosis is defined, and $CT\text{-}FFR_{auto}$ is automatically evaluated 20 mm distal to the beginning of the hemodynamically defined stenosis. Abbreviations: ΔCT-FFR, difference of computed tomography derived fractional flow reserve over a stenosis.

Figure 3. Bland Altman plot (A) and correlation (B) of $CT\text{-}FFR_{atloc}$ compared to invasive FFR in 175 lesions. The red dotted lines indicate cut-off values (≤0.80) for invasive FFR and CT-FFR.

Figure 4. ROC curve analysis of diagnostic performance of CT-FFR at three different sites (CT-$FFR_{atloc,\ auto\ and\ distal}$) and CCTA at per lesion (A) and per patient level (B).

ROC curve analysis for 175 lesions in 108 patients comparing the AUC for CT-FFR_{atloc}, CT-FFR_{auto}, CT-FFR_{distal} and CCTA, using invasive FFR ≤0.80 as gold standard.

Figure 5. Diagnostic accuracy, sensitivity, specificity, PPV and NPV of CCTA, CT-FFR_{atloc}, CT-FFR_{auto} and CT-FFR_{distal} at per patient level. Results are presented with 95% confidence intervals. Abbreviations: PPV, positive predictive value; NPV, negative predictive value.

Figure 6. PPV and NPV of CT-FFR_{atloc}, CT-FFR_{auto}, CT-FFR_{distal} and CCTA at per lesion (A) and per patient (B) level for low-to-intermediate and high CAC score group. Per lesion level: Low-to-intermediate CAC score group, n = 53, high CAC score group, n = 64. Per patient level: Low-to-intermediate CAC score group, n = 38, high CAC score group, n = 28.

Table 1. Baseline patient characteristics.

Variable	Value
Age, years	62 ± 8
Male	76 (67)
Time from CCTA to ICA, days	35 ± 15
DLP_{ccta}, $mGy^{x}cm$	195 ± 222
Effective CCTA radiation dose, mSv	5.1 ± 5.8

BMI, kg/m^2	27.5 ± 3.5
Height, cm	175 ± 9
Weight, kg	85 ± 16
Heart rate, bpm	67 ± 13
Systolic blood pressure, mmHg	143 ± 19
Diastolic blood pressure, mmHg	84 ± 9
Mean arterial pressure, mmHg	103 ± 12
Pretest probability of CAD, ESC 2019	23 ± 12
Agatston score, median (IQR, range)	
All (n=66)	263 (96-460, 0-1711)
Low-to-intermediate, 0-299 (n=38)	113 (24-156, 0-290)
High, ≥300 (n=28)	518 (375-810, 317-1711)
Risk factors	
Smoker/ former smoker	58 (51)
Hypertension	57 (50)
Dyslipidemia	50 (44)
Family predisposition	38 (33)
Diabetes	16 (14)
Previous cardiovascular disease	
Previous CAD events	1 (1)
TIA/stroke	10 (9)
Comorbidity	
COPD/asthma	2 (2)
Atrial fibrillation	8 (7)
Classification of angina	

Non anginal chest pain	16 (14)
Atypical	54 (47)
Typical	44 (39)
Medications	
β-blocker	24 (21)
Calcium antagonists	14 (12)
Nitrates	19 (17)
ACE inhibitor or ARB	39 (34)
Aspirin/another platelet inhibitor	97 (85)
Statin/ another lipid-modifying agent	98 (86)

Values are reported as frequency (%) when categorical data or mean ± SD when continuous variables unless otherwise specified.

Table 2. Vessel characteristics.

Variable	Value
Patients, n	108
Lesions, n	175
FFR positive patients	53 (49)
FFR positive lesions	83 (42)
Lesion location	
RCA (segment 1, 2, 3)	42 (1, n = 11, 2, n = 24, 3, n = 7)
LM/ LAD (Segment 5, 6, 7, 8, 9, 10)	108 (5, n = 3, 6, n = 32, 7, n = 33, 8, n = 20, 9, n = 17, 10, n = 3)
CX (Segment 11, 12, 13, 14, 17)	47 (11, n = 17, 12, n = 11, 13, n = 10, 14, n = 5,

	17, n = 4)
FFR	0.79 ± 0.13
$CT\text{-}FFR_{atloc}$	0.82 ± 0.13
$CT\text{-}FFR_{auto}$	0.86 ± 0.13
$CT\text{-}FFR_{distal}$	0.76 ± 0.12
CCTA	
1% - 24 % diameter stenosis	34 (19)
25% - 49 % diameter stenosis	36 (21)
50% - 69 % diameter stenosis	58 (33)
70% - 99 % diameter stenosis	47 (27)
FFR positive lesions	
Main vessel	70 (84)
Side branch	13 (16)
Functional 1-vessel disease	34 (64)
Functional 2-vessel disease	16 (30)
Functional 3 vessel disease	3 (6)

1 Values are reported as frequency (%) when categorical or mean ± standard deviation when
2 continuous variables unless otherwise specified.

3

Table 3. Diagnostic performance of CT-FFR and CCTA per lesion and per patient with invasive FFR as reference standard. FFR ≤0.80, CT-FFR ≤0.80 and CCTA ≥50% are used as cut-off limits.

	At patient level				At lesion level			
	$CT\text{-}FFR_{atloc}$	$CT\text{-}FFR_{auto}$	$CT\text{-}FFR_{distal}$	CCTA	$CT\text{-}FFR_{atloc}$	$CT\text{-}FFR_{auto}$	$CT\text{-}FFR_{distal}$	CCTA
TP, n	41	37	51	46	53	45	69	63
FP, n	9	8	28	33	13	10	42	55
TN, n	46	47	27	22	101	104	72	59
FN, n	12	16	2	7	30	38	14	20
Accuracy, %	81 (72-88)	78 (69-85)	72 (63-80)	63 (53-72)	78 (72-84)	76 (69-81)	72 (65-78)	62 (55-69)
Sensitivity, %	77 (64-88)	70 (56-82)	96 (87-100)	87 (75-95)	64 (53-74)	54 (43-65)	83 (73-90)	76 (65-85)
Specificity, %	84 (71-92)	86 (73-94)	49 (35-63)	40 (27-54)	89 (81-94)	91 (84-96)	63 (54-72)	52 (42-61)
PPV, %	82 (71-89)	82 (70-90)	65 (58-70)	58 (52-64)	80 (70-87)	82 (71-89)	62 (56-68)	53 (48-59)
NPV, %	79 (70-87)	75 (66-82)	93 (77-98)	76 (59-87)	77 (72-82)	73 (68-78)	84 (76-89)	75 (66-82)
AUC	0.87 (0.80-0.93)	0.86 (0.78-0.92)	0.83 (0.75-0.90)	0,74 (0.65-0.82)	0.83 (0.77-0.88)	0.81 (0.75-0.87)	0.78 (0.71-0.84)	0.65 (0.58-0.72)

Numbers in parentheses indicate the 95% confidence interval. Abbreviations: TP, true positive; FP, false positive; TN, true negative; FN, false negative; PPV, positive predictive value; NPV, negative predictive value; AUC, area under the curve.

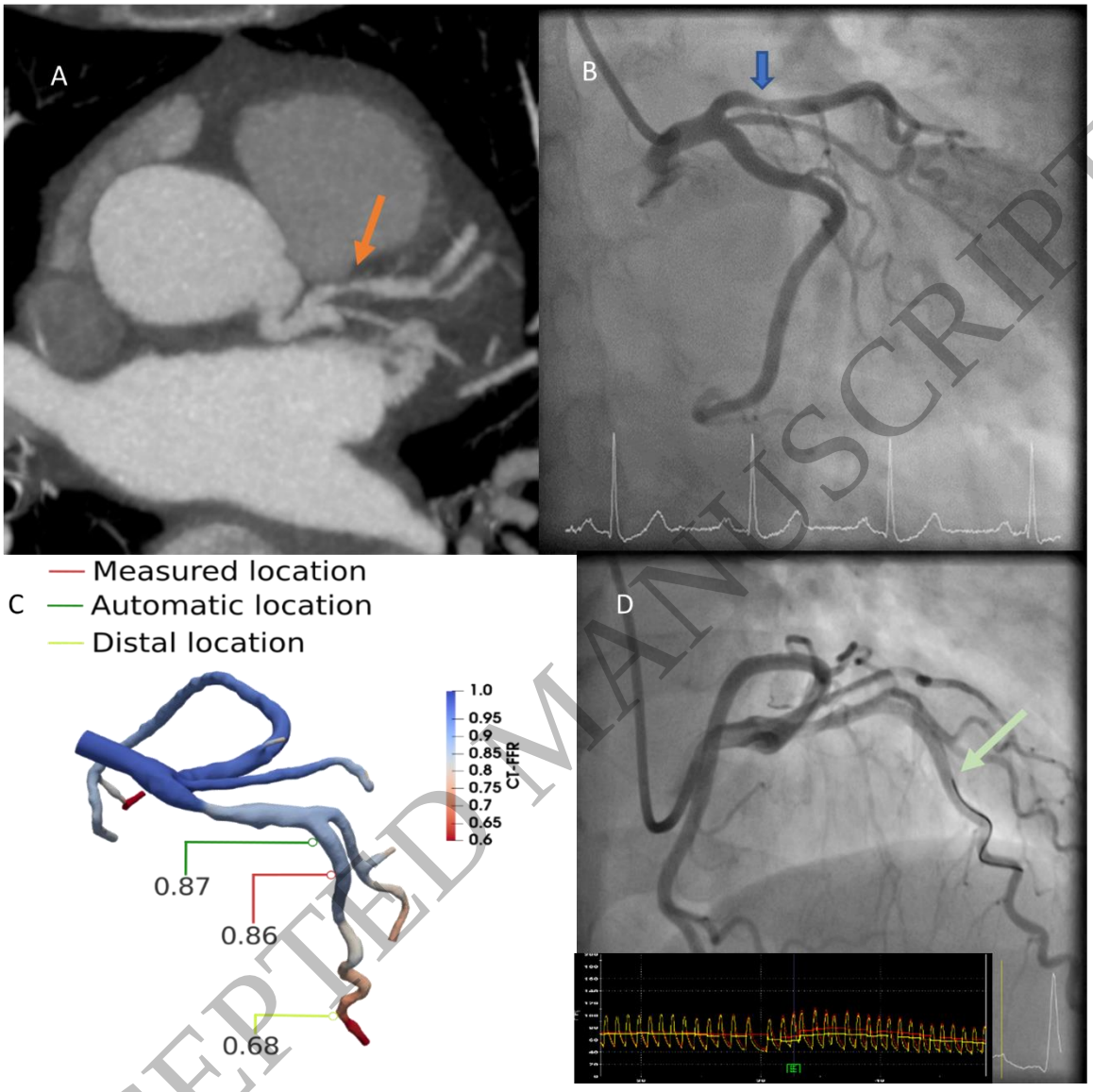

Figure 1
155x152 mm (x DPI)

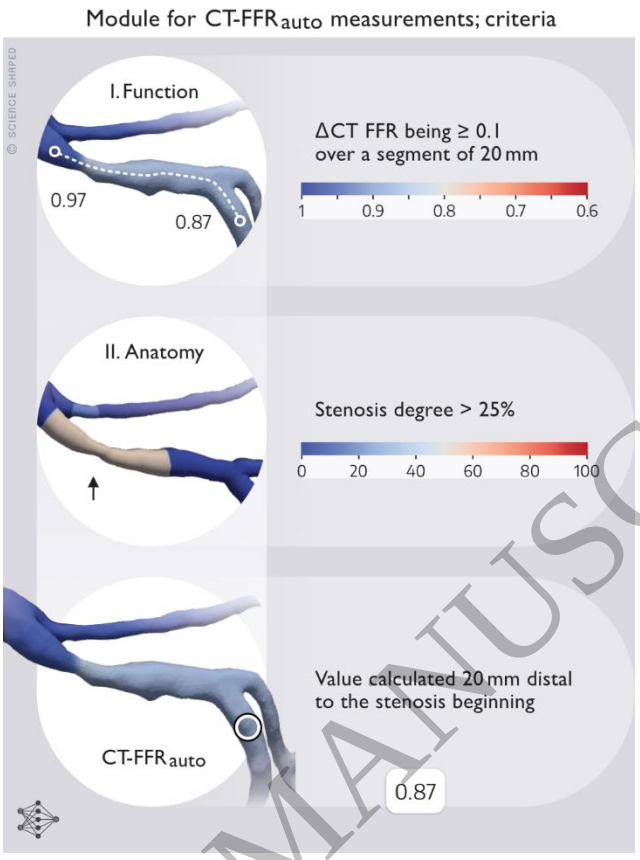

Figure 2
84x113 mm (x DPI)

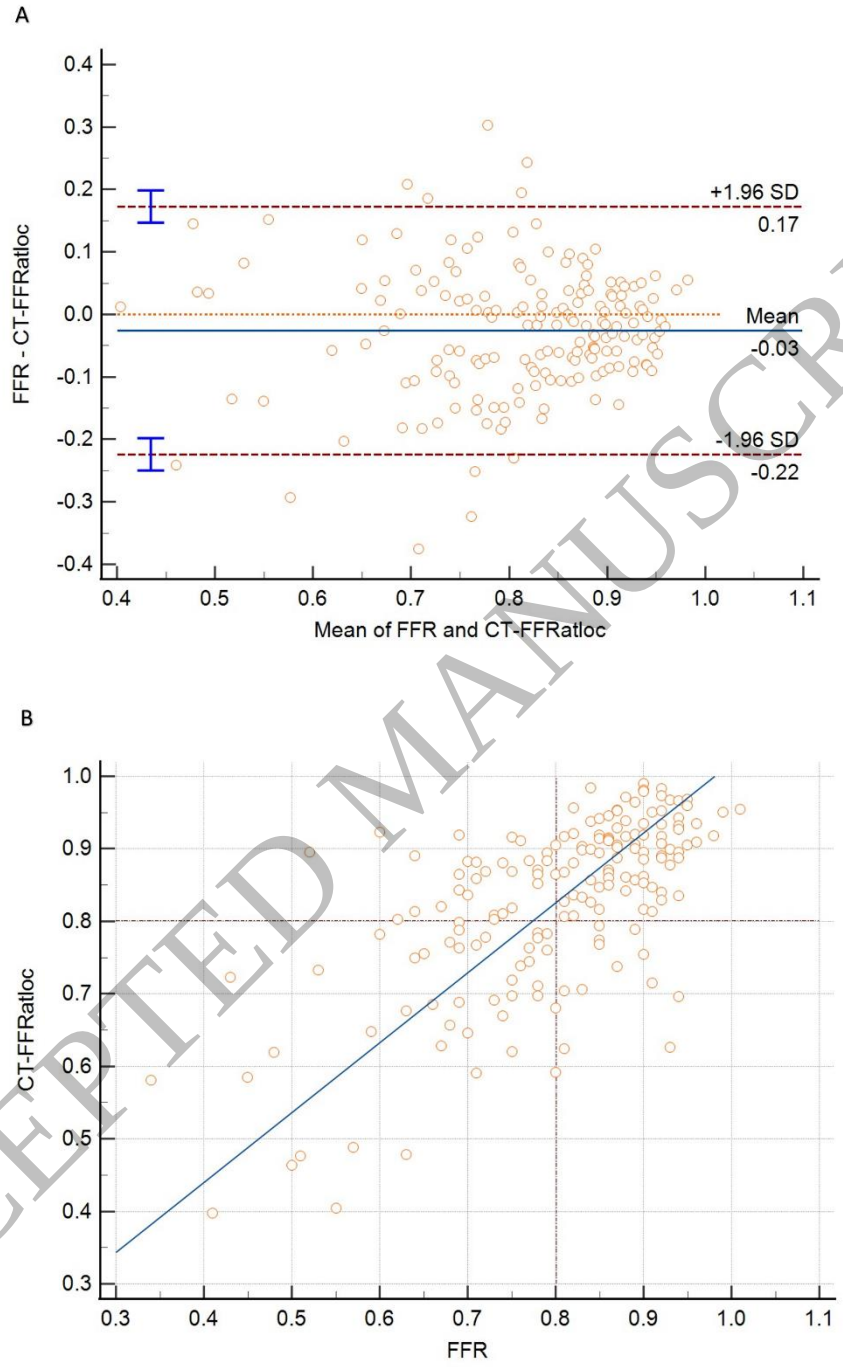

Figure 3
152x230 mm (x DPI)

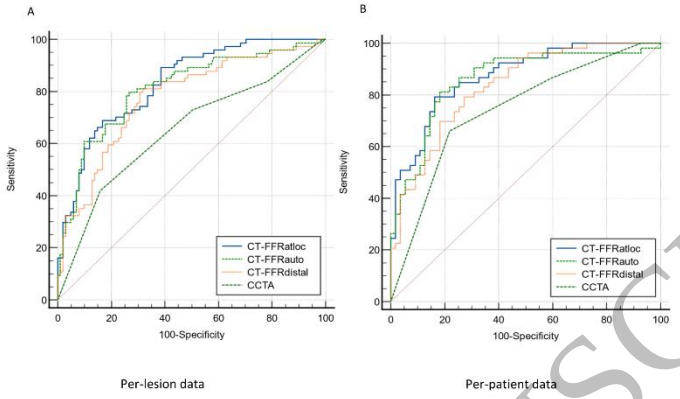

Figure 4
78x55 mm (x DPI)

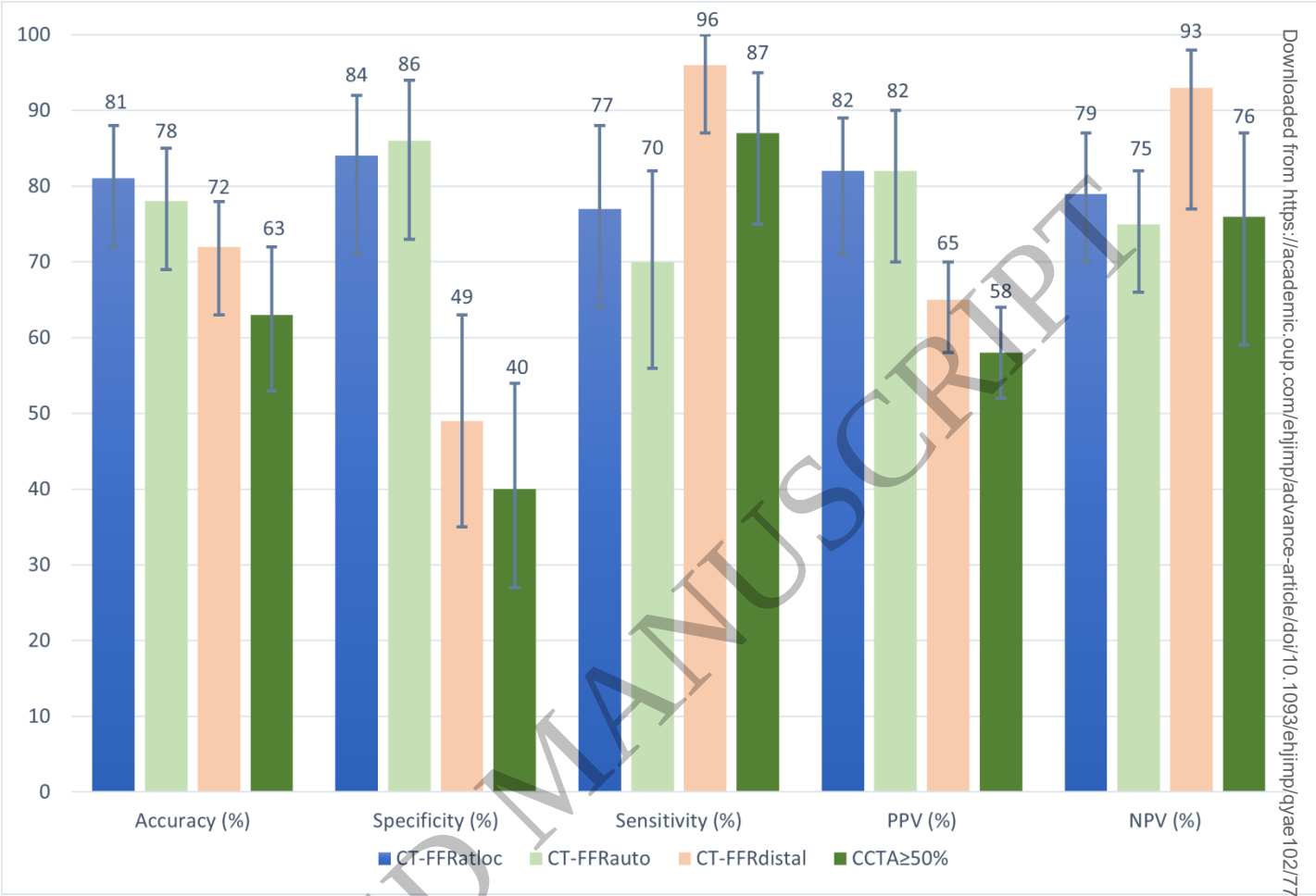

Figure 5
188x128 mm (x DPI)

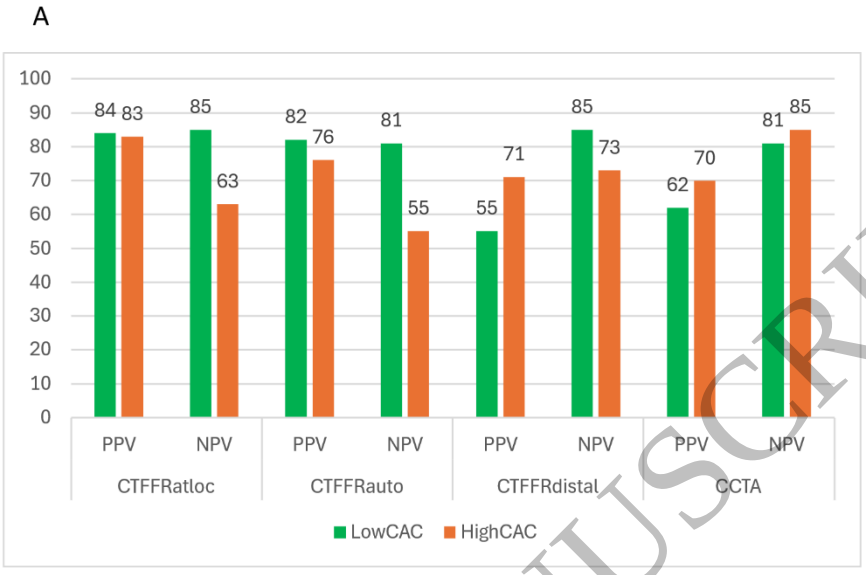

Per-lesion level

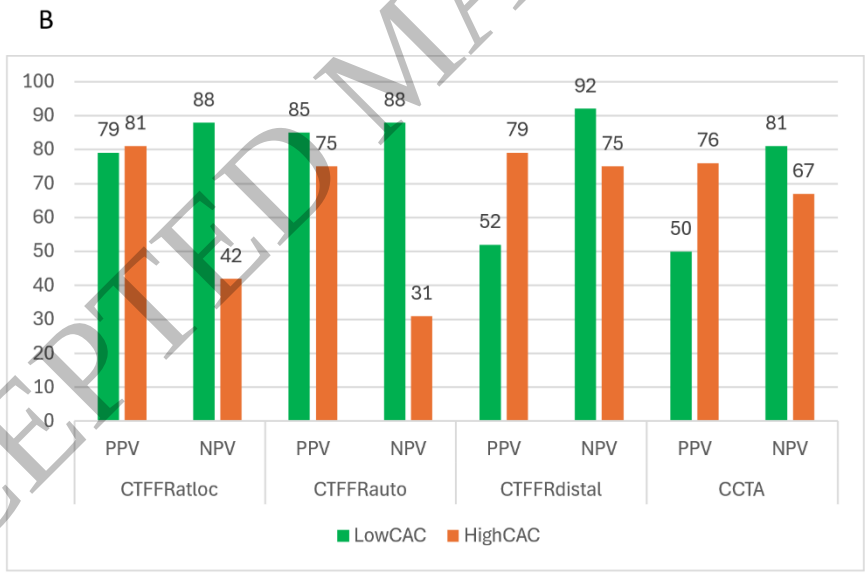

Per-patient level

Figure 6
118x203 mm (x DPI)

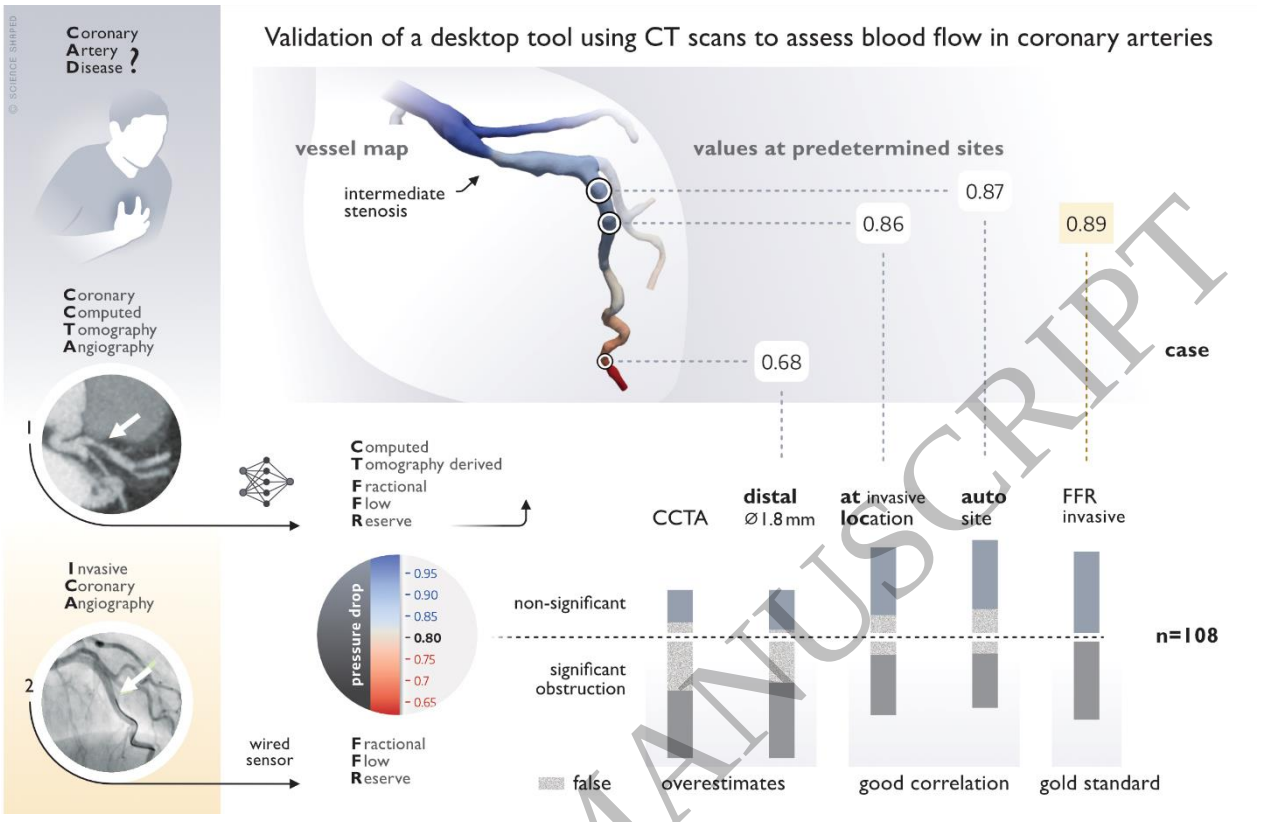

Graphical Abstract

Lead author biography

Anders T. Bråten serves as a cardiologist at St. Olavs University Hospital, Trondheim, Norway, and is a PhD candidate at the Norwegian University of Science and Technology. His research focuses on linking clinical practice to advanced imaging methods, particularly exploring coronary physiology in innovative CT based techniques, such as CT-FFR. A main focus of his research is to improve non-invasive diagnostics of coronary artery disease with the aim of reducing unnecessary invasive investigations.